Nuclear Physics B79 (1974) 259–275. North-Holland Publishing Company

DIFFRACTION DISSOCIATION OF NEUTRONS IN THE REACTION $dp \to ppp\pi^-$ AT 25 GeV/c ‡

J.W. COOPER, A.A. SEIDL and J.C. VANDER VELDE
The University of Michigan, Ann Arbor, Michigan 48104

Received 11 March 1974
(Revised 4 June 1974)

Abstract: We observe the reaction $dp \to p_{spec}(p\pi^-)p$ in a bubble chamber exposure at 25 GeV/c incident deuteron momentum. The $(p\pi^-)$ system with invariant mass below 2.0 GeV is interpreted as neutron diffraction dissociation. The $(p\pi^-)$ mass spectra show little if any direct evidence of N^* production. The decay angular distributions and the momentum transfer distributions of the $(p\pi^-)$ system suggest a smooth increase in contributions from higher partial waves ($J \geqslant \frac{3}{2}$) with increased mass or momentum transfer. A simple partial-wave analysis shows a P_{11} contribution below 1.3 GeV for small $-t'$ and a dominant D_{13} contribution elsewhere. Both the P_{11} and D_{13} amplitudes peak far below the $N^*(1470)$ and $N^*(1520)$ resonances. We also find evidence for the charge-exchange reaction $np \to p(p\pi^-)$. In this process the $(p\pi^-)$ system shows evidence for $\Delta^0(1236)$ and $N^*(1520)$ production.

1. Introduction

We report on a study of the reaction

$$dp \to pp\pi^-p \tag{1}$$

or, interpreting the neutron in the deuteron as free,

$$np \to p\pi^-p \tag{2}$$

at 25 GeV/c incident deuteron momentum in the Brookhaven National Laboratory 80-inch hydrogen bubble chamber. The reason for our choice of a deuteron beam has been discussed elsewhere [1]. Viewed in the rest frame of the deuteron, this experiment is equivalent to 12.5 GeV/c protons on deuterium.

In sect. 2 we discuss the experimental procedure and give the cross section for neutron dissociation into $p\pi^-$. The main features of the data are described in sects. 3 and 4. In sect. 5 we present a partial-wave analysis of the $p\pi^-$ system and we make some concluding remarks in sect. 6.

‡ Work supported in part by the US Atomic Energy Commission.

2. Experimental procedure

The exposure consisted of 250 000 pictures in which all four prong events with a positive track of $\geqslant 8$ GeV/c and a proton of $\leqslant 1$ GeV/c were measured. The measurers imposed these cuts using an on-line three-point curvature measurement in one view, and the slow protons were identified through their predicted ionization from this measurement. Track reconstruction and kinematic fitting of the 27 000 events measured were done by TVGP and SQUAW respectively. 2 754 events had a three or four constraint fit to (1).

We identify the final state protons as follows: the spectator proton (p_s) is the slowest proton in the deuteron rest frame, the recoiling target proton (p_p) is the slowest proton in the lab, and the proton from the neutron dissociation (p_n) is the remaining proton. Fig. 1 illustrates this identification in the lab frame and shows the momentum separation of the three protons.

As evidence that our spectator identification is correct, we show in fig. 2 the p_s and p_n momenta in the deuteron rest frame. Since p_s is fast in the lab, we see spectators at all momenta in contrast to pd experiments which cannot see spectators below about 80 MeV/c. For p_s momenta less than 300 MeV/c, the distribution in fig. 2 is in fair agreement with that expected from the square of the Hulthén momentum-space wave function [2] with $\alpha = 45.5$ MeV/c and $\beta = 7\alpha$. A good agreement with the Hulthén distribution for p_s momenta less than 300 MeV/c is obtained using $\alpha = 57.0$ MeV/c (not shown). The excess of events above 300 MeV/c may be partly due to double scattering, and we therefore restrict the p_s momentum to be less than 300 MeV/c in the deuteron frame. This cut leaves a sample of 2 320 events.

A Monte-Carlo simulation of the data indicates that we confuse the protons p_s and p_n about 3% of the time in this sample. This reflects the fact that it is very unlikely to have *both* a fast spectator proton p_s *and* a slow proton p_n in the deuteron rest frame. The protons p_p and p_n are well separated in the lab frame and rarely confused.

The angular distribution of p_s in the deuteron frame for events with p_s momentum less than 300 MeV/c is shown in fig. 3. The angular distribution agrees with the curve shown in fig. 3 which is that of an isotropic distribution modified by the Möller flux factor [3]. For the following analysis we therefore consider these 2 320 events as our final sample of the reaction

$$np \rightarrow p_n \pi^- p_p \,. \tag{3}$$

We find a cross section of 757 ± 52 μb for reaction (3) with p_s momentum less than 300 MeV/c. This value includes corrections for the following effects:

(a) *Scanning efficiency.* The scanning efficiency was determined to be 87.5% from a second scan of 30% of the film. This correction was applied to the entire 250 000 pictures.

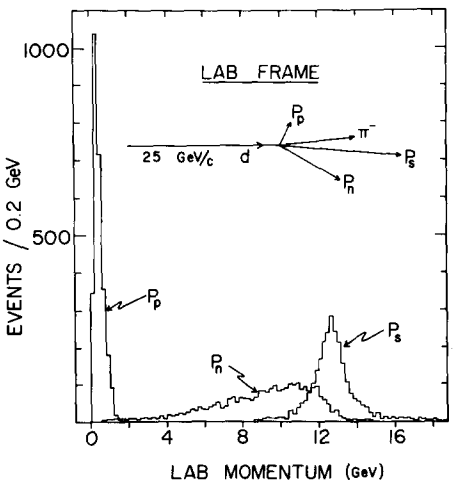

Fig. 1. Momentum vector diagram of a typical event in the lab, and the momentum distributions of the three protons in the lab. p_s is the spectator, p_p is the recoiling target, and p_n is the proton resulting from neutron dissociation.

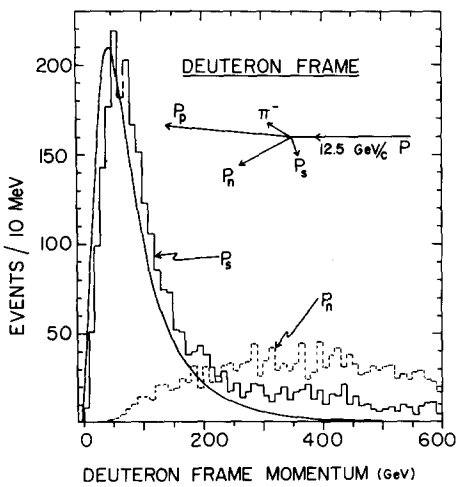

Fig. 2. Momentum vector diagram of a typical event in the deuteron rest frame, and the momentum distributions of p_s (spectator) and p_n in the deuteron rest frame. The curve is a Hulthén distribution with $\alpha = 45.5$ MeV/c, $\beta = 7.0\alpha$, normalized to 2 320 events.

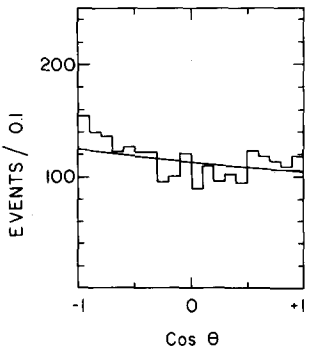

Fig. 3. The cosine of the angle between the spectator and the incident proton directions in the deuteron rest frame for events with p_s momentum < 300 MeV/c. The curve is the distribution expected in the spectator model, normalized to 2 320 events, and modified by the Möller flux factor.

(b) *Missed three prongs.* We extrapolate the distribution of $d\sigma/dt'$ *versus* $-t'$ to $-t' = 0$, and find a 6% loss due to protons which are too short to be seen *.

(c) *Glauber correction [4], [5].* A 6% correction is included for the loss of events when the neutron is shadowed by the proton in the deuteron.

(d) *Measurement failures.* 4.5% of the events were lost due to measurement failures.

(e) *Slow proton scan bias.* We estimate a 4% loss due to our requirement of a proton $\leqslant 1$ GeV/c.

The 52 μb error in the cross section reflects an additional 3.5% error above statistics due to the uncertainty in making the p_s momentum cut at 300 MeV/c. Our cross section for reaction (3) can be compared to 818 ± 75 μb found at 11.6 GeV/c (p on d) for the same reaction [6].

3. General features

The square of the four-momentum transfer t' ($t' = t - t_{min}$) from the target proton to p_p is shown in fig. 4. In the $-t'$ range of 0.02–0.5 GeV^2 this distribution can be adequately fit by an exponential

$$\frac{d\sigma}{dt'} = Ae^{bt'}, \tag{4}$$

in which $A = 4.3 \pm 0.2$ mb/GeV^2 and $b = 6.0 \pm 0.2$ GeV^{-2}. Extrapolating this fit to $-t' = 0$, we find we are missing approximately 140 events in the 0–0.02 GeV^2 $-t'$ range. These are events in which p_p is too short to be seen, and are the basis for our 6% cross section correction in sect. 2.

* This will be discussed in sect. 3.

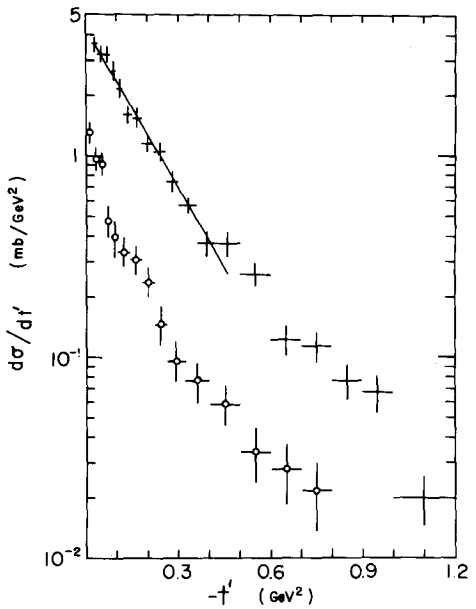

Fig. 4. (a) Differential cross section $d\sigma/dt'$ for all 2 320 events fitting reaction (3). $t' = t - t_{min}$ is the momentum transfer squared from the target proton to p_p. The curve corresponds to an exponential with slope 6 GeV^{-2}. (b) (open circles) $d\sigma/dt'$ for the 502 charge exchange events selected by the MIM test. t' is the momentum transfer squared from the incoming neutron to p_n.

The invariant masses $M(p_p\pi^-)$ and $M(p_n\pi^-)$ are shown in figs. 5a and 5b respectively. The experimental resolution in $M(p_n\pi^-)$ varies linearly from 5 to 20 MeV in the 1.2–1.8 GeV mass region. The resolution in $M(p_p\pi^-)$ varies from 5 to 10 MeV in the same region. The major feature of the $p_n\pi^-$ spectrum is a large broad enhancement in the 1.2–1.6 GeV region characteristic of a diffractive process. There is also some indication of a small peak near 1.7 GeV, but no other evidence for resonant peaks in the diffractively produced $p_n\pi^-$ system. A similar lack of resonance production has been noted with much higher statistics in $n \to p\pi^-$ off nuclear targets [7].

The $p_p\pi^-$ spectrum displays a small enhancement near 1.25 GeV and possibly some structure at 1.5 GeV. This low-mass structure indicates that at least some of our events involve pion production at the proton vertex in the charge-exchange process

$$np \to p_n(p_p\pi^-)\,, \tag{5}$$

rather than neutron dissociation in the process

$$np \to (p_n\pi^-)p_p\,. \tag{6}$$

The diagrams shown in fig. 6 illustrate these two reactions.

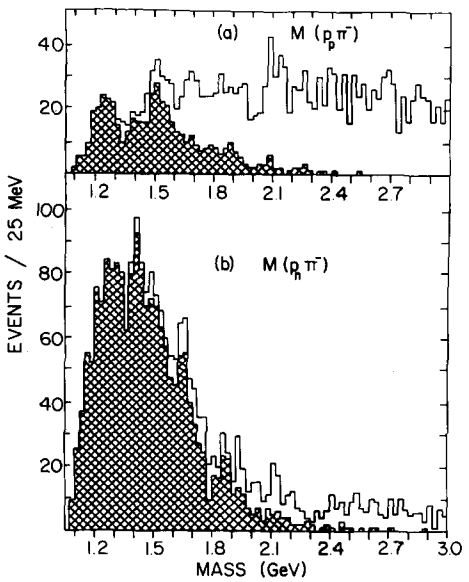

Fig. 5. (a) Invariant mass of the $p_p\pi^-$ system. The shaded histogram is for events with $M(p_p\pi^-) < M(p_n\pi^-)$. (b) Invariant mass of the $p_n\pi^-$ system. The shaded histogram is for events with $M(p_n\pi^-) < M(p_p\pi^-)$.

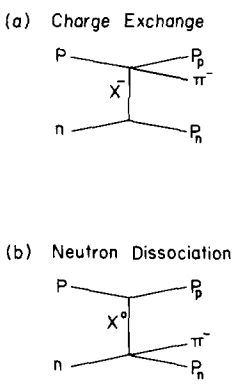

Fig. 6. (a) Charge exchange and (b) neutron dissociation diagrams contributing to the reaction $np \to pp\pi^-$.

The asymmetry between figs. 5a and b indicates the degree to which the reactions (5) and (6) can be separated at our energy. A more complete separation is obtained using the Minimum Invariant Mass (MIM) criterion of Yekutieli et al. [8]. The MIM test differentiates events for which $M(p_p\pi^-) < M(p_n\pi^-)$ (plotted in the shaded histogram of fig. 5a) from events for which $M(p_n\pi^-) < M(p_p\pi^-)$ (plotted in

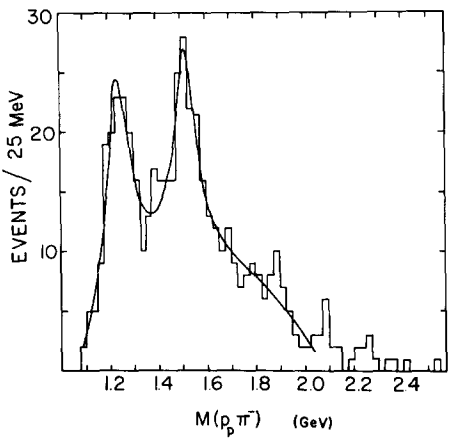

Fig. 7. Invariant mass of the $p_p\pi^-$ system for events with $M(p_p\pi^-) < M(p_n\pi^-)$. The curve is the fit described in the text with two Breit-Wigner resonances and a background.

the shaded histogram of fig. 5b). The 502 shaded events in fig. 5a would then be identified with the charge exchange reaction (5), while the remaining 1 818 shaded events in fig. 5b would correspond to neutron dissociation as in (6).

While such a mass selection cannot be completely reliable (as noted in ref. [9]), it does clarify the low-mass structure in the $p_p\pi^-$ spectrum. The mass plot in fig. 5a can now be described in terms of the $\Delta^0(1236)$, an N^* isobar with a peak near 1.5 GeV, and phase space. A fit using a linear combination of two Breit-Wigner intensities plus a background term dominated by phase space at low masses and damped by a polynomial at high masses gives the curve in fig. 7. The fitted Breit-Wigner resonance parameters and the cross sections for Δ^0 and N^* production corresponding to this curve are given in table 1. Evidence for $\Delta^0(1236)$, $N^*(1520)$ and $N^*(1688)$ resonance production in the charge exchange reaction has been reported previously in pd [6, 8, 10], and in np [9, 11] experiments. We note that equal amounts of $\Delta^0(1236)$ ($I=\frac{3}{2}$) production due to isovector exchange must appear in reactions (5) and (6), whereas one-fourth as much $N^*(1520)$ ($I=\frac{1}{2}$) production due to isovector exchange should appear in reaction (6) as in the charge-exchange reaction (5).

The differential cross section $d\sigma/dt'$ for the 502 charge exchange events selected by the MIM test is shown in fig. 4. In this case $-t'$ is the square of the four-momentum transfer from the incoming neutron to p_n. The distribution in fig. 4 is not well described by a simple exponential of type (4), as the slope b varies from 15 to 4 GeV^{-2} in the $-t'$ range 0–0.6 GeV^2.

The $M(p_n\pi^-)$ histogram is relatively unaffected by the MIM selection except for events in the high mass tail (see fig. 5b). The differential cross section $d\sigma/dt'$ is also unchanged (not shown) except for a scale factor. An exponential fit of type (4) yields $A = 3.6 \pm 0.2$ mb/GeV^2 and $b = 6.5 \pm 0.3$ GeV^{-2}.

Table 1
Breit-Wigner resonance parameters and N* cross sections for the fit to the invariant mass plot $M(p_p\pi^-)$ (MIM selection) of fig. 7. The cross sections are quoted for the reaction $np \to p_n N^* \to p_n p_p \pi^-$ and include a correction for the MIM cut.

	M_0(MeV)	Γ(MeV)	Cross section (μb)
$\Delta^0(1236)$	1231 ± 11	109^{+32}_{-25}	35 ± 7
$N^*(1520)$	1515 ± 11	106^{+39}_{-33}	42 ± 10

The data therefore indicate that neutral isovector exchange contribution to the low-mass enhancement in fig. 5b is small (< 9%), and that the tail due to the charge-exchange contribution from reaction (5) is also small. Thus for $M(p_n\pi^-)$ less than about 2.0 GeV we are looking primarily at isoscalar meson exchange and/or pomeron exchange giving rise to diffraction dissociation of neutrons into $p\pi^-$. The remainder of the paper will deal with the $p_n\pi^-$ system in all 2 320 events fitting reaction (3) with p_s momentum less than 300 MeV/c (no MIM selection).

The $M(p_n\pi^-)$ mass spectra are shown for $-t' < 0.1$ and $-t' > 0.1$ GeV^2 in fig. 8. In both cases the main feature is the broad low-mass enhancement, but the central value of this peak is shifted to a higher value for the higher $-t'$ region. A similar behaviour has been seen in pd [8], K^+d [12], and π^-d [13] experiments. We see no good evidence for increased resonance production near 1.5 and 1.7 GeV at high $-t'$, in contrast to the experiments mentioned.

We have also examined the differential cross section $d\sigma/dt'$ for different $p_n\pi^-$ mass regions. In each mass bin we fit the distribution to the exponential form (4), and in fig. 9 we show the resulting slope b. The slope is about 15 GeV^{-2} near threshold and decreases smoothly to around 5 GeV^{-2} near 1.6 GeV. Similar changes in slope with increasing $p\pi^-$ mass have been reported in other experiments observing neutron diffraction dissociation [8, 11, 12, 13]. In fact this feature is common to most diffractive processes, and Miettinen and Pirilä [14] have shown that this cannot be explained as being simply due to kinematics in the context of a Deck effect or of a multiperipheral model.

In fig. 10 we present the differential cross section for four different regions of $p_n\pi^-$ mass to show the slope change discussed above and to show the change in the *shape* of the distributions. In the lowest mass bin there is a definite break in the slope at a $-t'$ of about 0.25 GeV^2. For $1.3 < M(p_n\pi^-) < 1.45$ GeV, there is no break, and a single exponential provides an excellent description of the data. In the two higher mass bins there is a suggestion that the distributions flatten out at small $-t'$. It has been suggested by Kane [15] that this behaviour can be naturally described in terms of s-channel helicity amplitudes where an amplitude of net helicity flip n contains a t' dependence like $J_n(R\sqrt{-t'})$. In this picture our low mass bin in fig. 10 would have a large $n = 0$ contribution. In fact the differential cross section just above threshold

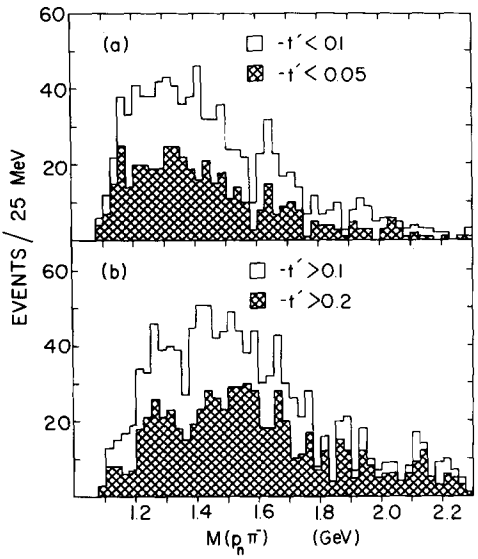

Fig. 8. The invariant mass $M(p_n\pi^-)$ for events with (a) $-t' < 0.1$ GeV^2 (shaded events have $-t' < 0.05$ GeV^2) and (b) $-t' > 0.1$ GeV^2 (shaded events have $-t' > 0.2$ GeV^2).

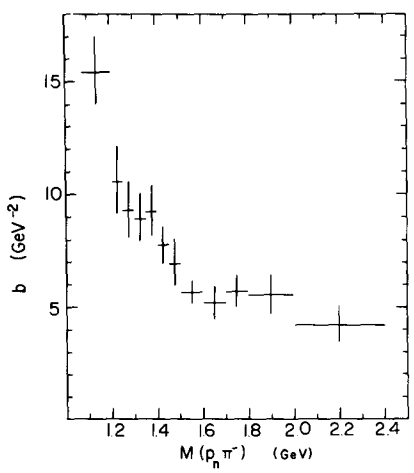

Fig. 9. Slope-mass correlation for $np \to (p_n\pi^-)p_p$. The slope b is determined by fitting the differential cross section $d\sigma/dt'$ to the form $A\,e^{bt'}$ in each mass bin. The $-t'$ range fit in each bin varies from 0.02–0.3 GeV^2 near threshold to 0.05–0.6 GeV^2 in the higher mass bins in order to accomodate the *shapes* seen in figs. 10 and 11.

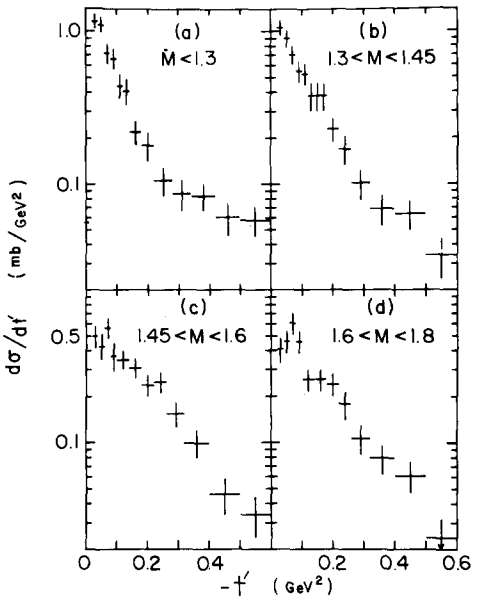

Fig. 10. $d\sigma/dt'$ *versus* $-t'$ for four ranges of $p_n\pi^-$ mass, (a) $M(p_n\pi^-) < 1.3$ GeV, (b) $1.3 < M(p_n\pi^-) < 1.45$ GeV, (c) $1.45 < M(p_n\pi^-) < 1.6$ GeV, and (d) $1.6 < M(p_n\pi^-) < 1.8$ GeV.

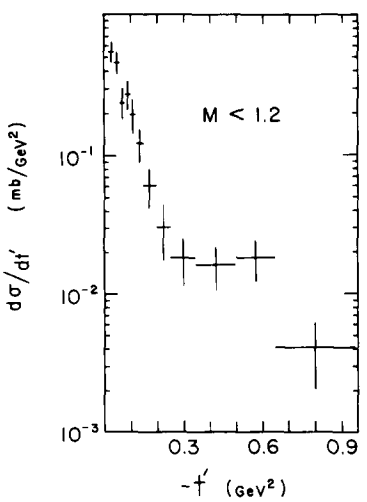

Fig. 11. $d\sigma/dt'$ *versus* $-t'$ for $M(p_n\pi^-) < 1.2$ GeV.

($M(p_n\pi^-) < 1.2$ GeV) shows the dip expected in a J_0 description (see fig. 11). The 1.3–1.45 GeV region in fig. 10 would contain roughly equal amounts of $n = 0$ and $n = 1$ amplitudes, and the decrease in slope near $-t' = 0$ in the higher mass bins would imply the onset of larger $n > 0$ contributions.

4. Angular distributions

Angular momentum information about the $p_n\pi^-$ system can be obtained from the decay angles of the proton in the Gottfried-Jackson and helicity frames defined in the $p_n\pi^-$ c.m. In the Gottfried-Jackson frame the $\hat{z}_J$ axis is defined along the direction of the neutron and the $\hat{y}_J$ axis is perpendicular to the production plane ($\hat{y}_J = \overrightarrow{\text{target} \times p_p}$). In the helicity frame the $\hat{z}_H$ axis is defined as opposite to the direction of p_p, and $\hat{y}_H = \hat{y}_J$. The cosine of the polar angle $\cos\theta_J$ and the azimuthal angle ϕ_J in the Gottfried-Jackson frame are shown in fig. 12. $\cos\theta_H$ and ϕ_H in the helicity frame are shown in fig. 13.

The $\cos\theta_J$ distribution for low-mass and low-momentum transfer (fig. 12a) is fairly isotropic but does peak towards $\cos\theta_J = +1$. The corresponding ϕ_J distribution is definitely anisotropic. Since we expect both $\cos\theta_J$ and ϕ_J to be flat for a pure $J = \frac{1}{2}$ state of the $p_n\pi^-$ system, the simplest interpretation of the data would include the presence of higher partial waves ($J \geqslant \frac{3}{2}$). Comparing figs. 12(a) and (c), $\cos\theta_J$ in the low $-t'$ range shows increasing forward and backward peaks with an increased forward-backward asymmetry for higher $p_n\pi^-$ mass. In the high $-t'$ range the distributions in the two mass regions are very similar to one another (figs. 12(b) and (d)). Comparing fig. 12(a) with (b) and (c) with (d), we again see a larger asymmetry peaked towards $\cos\theta_J = +1$ as $-t'$ increases in each mass range. This behaviour can be described in terms of a smooth increase in contributions from higher partial waves with increased mass or momentum transfer.

Other experiments indicate a similar picture but disagree in detail. In π^-d interactions at 15 GeV/c [13] $\cos\theta_J$ is fairly isotropic for low $p\pi^-$ mass at both low and high values of momentum transfer. Their $\cos\theta_J$ distributions for high $p\pi^-$ mass are very similar to ours. In neutron diffraction dissociation off carbon at 20–30 GeV/c [16] a backward peak is seen for all masses and $-t' < 0.3$ GeV^2 ‡.

Another view of the angular momentum information the $p_n\pi^-$ system is provided by examining the mean values of the spherical harmonics Y_l^m as a function of $M(p_n\pi^-)$. The Gottfried-Jackson angles (θ_J, ϕ_J) of the proton p_n are used to calculate $\langle Y_l^m \rangle$. The $\langle Y_l^0 \rangle$ with $1 \leqslant l \leqslant 6$ are shown for events with $-t' < 0.1$ GeV^2, for events with $-t' > 0.1$ GeV^2, and for all events in figs. 14, 15 and 16, respectively. In all cases the distributions start at a value near zero at threshold and rise to some positive value at higher mass. This is the behaviour one expects if higher partial waves become more important for higher masses.

‡ The experiment of ref. [16] only detects the π^- in the hemisphere we call $-1 < \cos\theta_J < 0$. Note they define θ as the angle of the π^- instead of the proton.

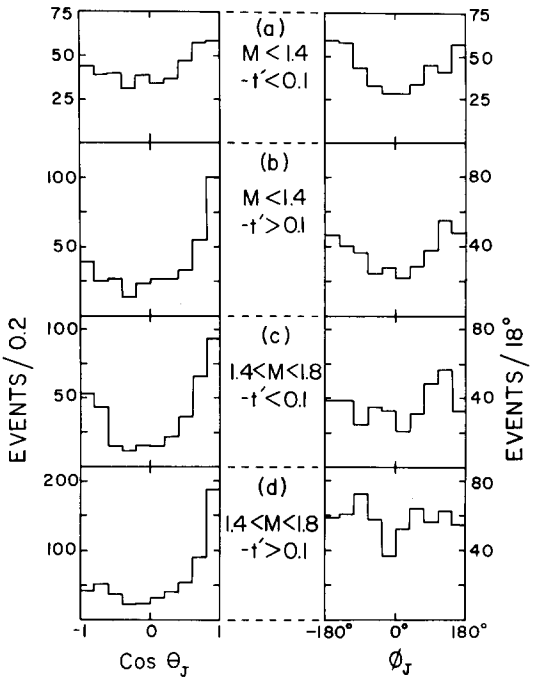

Fig. 12. Distributions in $\cos\theta_J$ and ϕ_J for the proton p_n in the Gottfried-Jackson frame for (a) $-t' < 0.1$ GeV^2 and $M(p_n\pi^-) < 1.4$ GeV, (b) $-t' > 0.1$ GeV^2 and $M(p_n\pi^-) < 1.4$ GeV, (c) $-t' < 0.1$ GeV^2 and $1.4 < M(p_n\pi^-) < 1.8$ GeV, and (d) $-t' > 0.1$ GeV^2 and $1.4 < M(p_n\pi^-) < 1.8$ GeV.

In particular the $\langle Y_l^0 \rangle$ for $l \geqslant 3$ increase significantly near 1.7 GeV and suggest the strong onset of higher waves at that point. $\langle Y_1^0 \rangle$ and $\langle Y_2^0 \rangle$ show differences in behaviour for low $-t'$ (figs. 14a, b) and high $-t'$ (figs. 15a, b) in that both distributions take on significantly larger values in the high $-t'$ region for masses below 1.5 GeV. As in the $\cos\theta_J$ distributions (fig. 12), this indicates the dominance of $J \geqslant \frac{3}{2}$ states for all but the lowest mass and momentum transfer region. The $\langle Y_l^0 \rangle$ values in figs. 14 and 15 are very similar to those observed by Lissauer et al. in K^+d at 12 GeV/c [12]. The $\langle Y_l^0 \rangle$ values in fig. 16 (no t' cut) agree with those reported by Ansorge et al. in np at 5.5–8.0 GeV/c [9].

The real parts of $\langle Y_l^m \rangle$ for $l \leqslant 3$ and $1 \leqslant m \leqslant l$ are shown in fig. 17. $\langle Y_1^1 \rangle$ and $\langle Y_2^1 \rangle$ show small but significant positive peaks near $M(p_n\pi^-) = 1.35$ GeV. $\langle Y_3^1 \rangle$ is also positive in this region, and both $\langle Y_2^1 \rangle$ and $\langle Y_3^1 \rangle$ show some evidence for another peak near 1.9 GeV. Non-zero values of these moments have also been reported by Yekutieli et al. [8]. It is not clear if this behaviour could be explained by interference effects due to the presence of the small $\Delta^0(1236)$ contribution in our sample.

The imaginary parts of the $\langle Y_l^m \rangle$ for $m \neq 0$ (not shown) are consistent with zero for all mass and momentum transfer regions as expected from parity conservation.

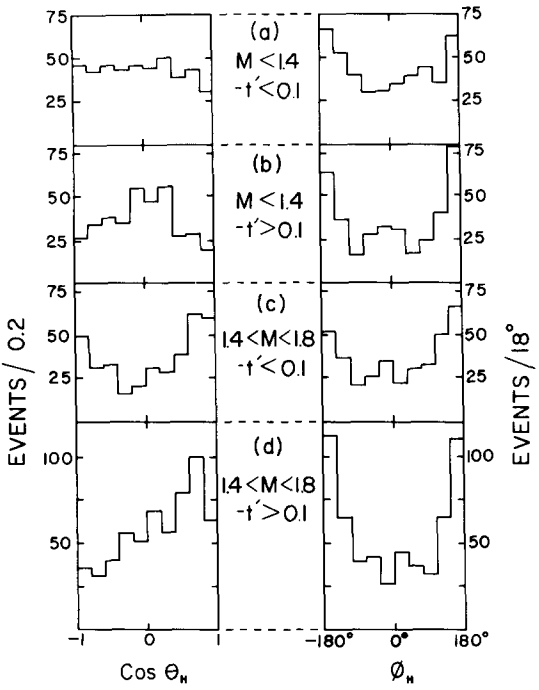

Fig. 13. Distributions in $\cos\theta_H$ and ϕ_H for the proton p_n in the helicity frame for (a) $-t' < 0.1$ GeV^2 and $M(p_n\pi^-) < 1.4$ GeV, (b) $-t' > 0.1$ GeV^2 and $M(p_n\pi^-) < 1.4$ GeV, (c) $-t' < 0.1$ GeV^2 and $1.4 < M(p_n\pi^-) < 1.8$ GeV, and (d) $-t' > 0.1$ GeV^2 and $1.4 < M(p_n\pi^-) < 1.8$ GeV.

5. Partial-wave analysis

We have done a simple partial-wave analysis of the $\langle Y_l^0 \rangle$ distributions in terms of a model containing only P_{11}, D_{13}, and F_{15} wave amplitudes, corresponding to $J^P = \frac{1}{2}^+, \frac{3}{2}^-, \frac{5}{2}^+$ respectively. Specifically, we fix the mass dependence and phase of the F wave to be that of a Breit-Wigner of mass 1 688 MeV and width 130 MeV. The F-wave normalization is fixed by the number of events observed in the 1.7 GeV region in the mass plot. The D-wave phase is chosen as a Breit-Wigner of mass 1 520 MeV and width 120 MeV, and the D-wave magnitude is left free as a parameter in each mass bin. The P-wave phase and magnitude are both free parameters in each bin. In each mass bin for $M(p_n\pi^-) < 1.775$ GeV we fit to the mass population and to the observed values of $\langle Y_l^0 \rangle$ for $1 \leqslant l \leqslant 4$. This analysis is patterned after the analysis of Lissauer et al. [12]. The $\langle Y_l^0 \rangle$ can be found in ref. [12] expressed in terms of P, D, and F-wave amplitudes.

For $-t' < 0.1$ GeV^2 we fit simultaneously the $M(p_n\pi^-)$ spectrum of fig. 8a and the $\langle Y_l^0 \rangle$ of fig. 14 in each of the fourteen 50 MeV mass bins below 1.775 GeV. The average χ^2 probability for these fits is 37%. The partial-wave analysis shows that the

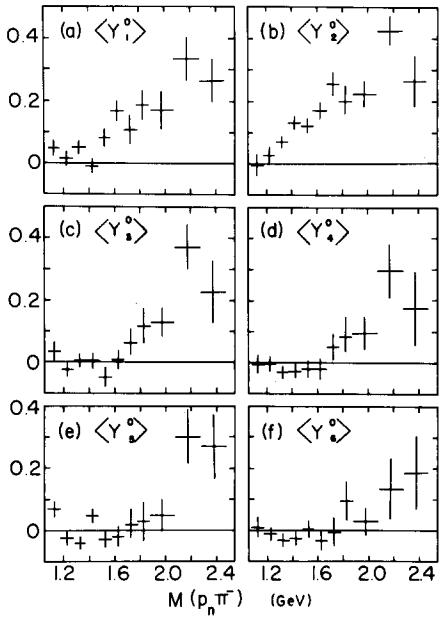

Fig. 14. Values of $\langle Y_l^0 \rangle$ as a function of $M(p_n\pi^-)$ for events with $-t' < 0.1$ GeV^2.

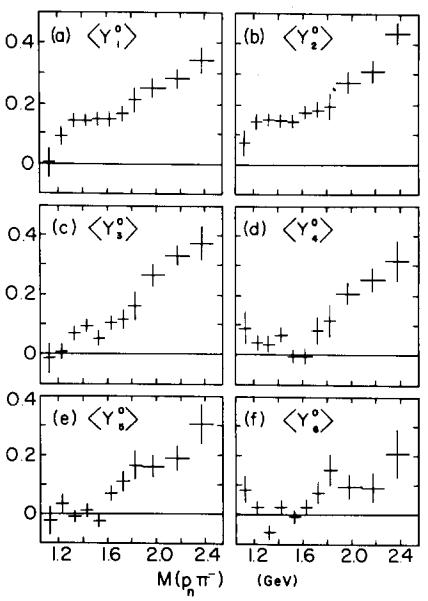

Fig. 15. Values of $\langle Y_l^0 \rangle$ as a function of $M(p_n\pi^-)$ for events with $-t' > 0.1$ GeV^2.

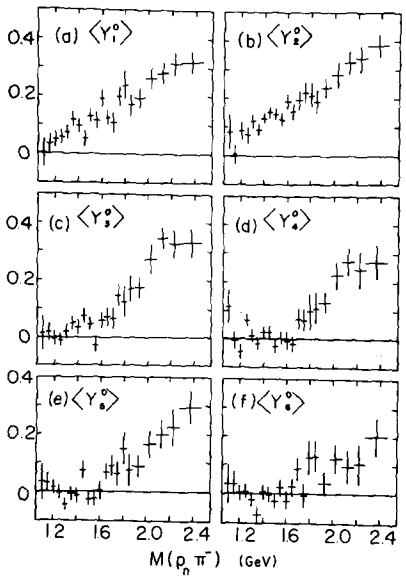

Fig. 16. Values of $\langle Y_l^0 \rangle$ as a function of $M(p_n\pi^-)$. No cut has been made on the momentum transfer $-t'$.

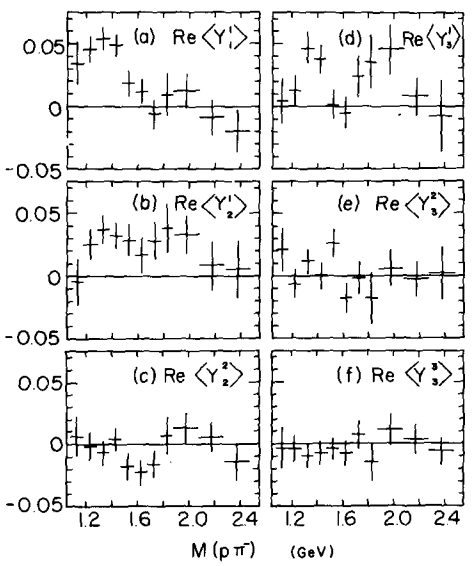

Fig. 17. Values of the real part of $\langle Y_l^m \rangle$ as a function of $M(p_n\pi^-)$.

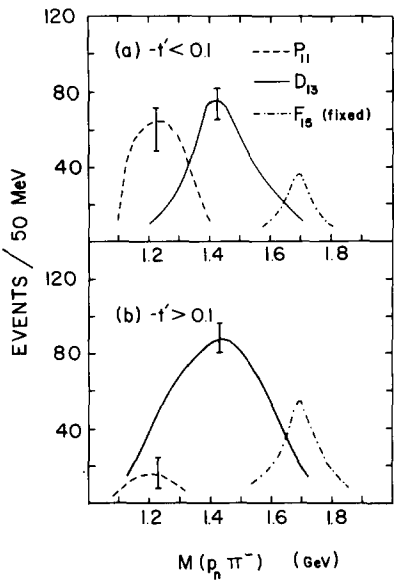

Fig. 18. Approximate shapes and sizes of the P_{11}, D_{13}, and F_{15} wave contributions to the $p_n\pi^-$ mass spectrum for (a) $-t' < 0.1$ GeV^2 and (b) $-t' > 0.1$ GeV^2.

data can be described by the approximate P- and D-wave contributions shown in fig. 18a. The P-wave phase is determined by P-D interference in $\langle Y_1^0 \rangle$ and is found to be near 90° ‡ in the 1.2–1.35 GeV region. The fits are insensitive to the P-wave phase elsewhere due to the small overlap of the P and D amplitudes. The fits are also insensitive to our choice of the D-wave phase. The average χ^2 probability remains near 35% in fits with a Breit-Wigner D-wave phase of larger width and lower central value, in fits with the phase equal to zero, and in fits with the phase as a free parameter. We do consistently find the P-wave phase to lead the D-wave phase by about 90° in the 1.2–1.35 GeV region.

We find a much smaller P-wave contribution than was reported in the K^+d experiment [12]. Over half of our event population is accounted for by the D wave. The P and D wave *shapes* in fig. 18a are very similar to those observed in ref. [12]. The P wave peaks about 200 MeV below the accepted value of the P_{11} $N^*(1470)$ resonance. The D wave peaks at about 1420 MeV, also lower than the D_{13} $N^*(1520)$, and the D wave state is much broader (~ 250 MeV) than the 105–150 MeV value found in phase-shift analyses [17].

If we now do the partial-wave analysis outlined above for the events with $-t' >$ 0.1 GeV^2, we find that the data can be completely described by D and F waves alone

‡ This value is determined relative to the D wave Breit-Wigner phase $\phi = \tan^{-1}\{\frac{1}{2}\Gamma/(M_0 - M)\}$ with $\Gamma = 120$ MeV and $M_0 = 1520$ MeV.

(see fig. 18b). The average χ^2 probability of the fits in this case is 13%. The lack of a significant P wave for $-t' > 0.1$ GeV^2 agrees with the results of ref. [12] and with our interpretation of the Gottfried-Jackson angular distributions in figs. 12a and 12c.

6. Conclusions

We have observed diffraction dissociation of neutrons into $p\pi^-$ in the reaction $dp \to p_s(p_n\pi^-)p_p$ with a cross section of about 0.76 mb. The $p_n\pi^-$ mass spectra show little if any direct evidence of N* production. The distributions in $t'(p \to p_p)$, and the angular distributions of the proton p_n all suggest a smooth increase in contributions to the $p_n\pi^-$ system from higher partial waves ($J \geqslant \frac{3}{2}$) with increased mass or momentum transfer. A simple partial-wave analysis in terms of P_{11}, D_{13}, and F_{15} amplitudes shows the D wave to be dominant with a small P-wave contribution for $M(p_n\pi^-) < 1.3$ GeV and $-t' < 0.1$ GeV^2. Both the P- and D-wave amplitudes found in this analysis peak lower than the accepted P_{11} N*(1470) and D_{13} N*(1520) resonances.

We also find evidence for the charge exchange reaction $dp \to p_s p_n(p_p\pi^-)$. In this case the $p_p\pi^-$ system shows evidence for production of the 1236 and 1520 N* resonances with cross sections of about 35 μb and 42 μb respectively.

We thank the aternating-gradient synchrotron staff and the 80-inch bubble chamber staff at Brookhaven National Laboratory for their help in obtaining this exposure. We are particularly indebted to H. Foelsche for help in obtaining the deuteron beam.

References

[1] J.W. Chapman et al., Phys. Rev. Letters 30 (1972) 64.
[2] L. Hulthén and M. Sugawara, Handbuch der Phys. 39 (1957) 1.
[3] Particle Data Group, Rev. Mod. Phys. 45 (1973) S1, p. 33.
[4] R.J. Glauber, Phys. Rev. 100 (1955) 242.
[5] Yu.P. Gorin et al., Yad. Fiz. 15 (1972) 953; Sov. J. Nucl. Phys. 15 (1972) 530.
[6] D. Hochman et al., Particle production in pn collisions at 11.6 GeV/c, Paper submitted to the 2nd Aix-en-Provence Conf. on elementary particles, September 1973.
[7] M.J. Longo et al., Phys. Letters 36B (1971) 560.
[8] G. Yekutieli et al., Nucl. Phys. B40 (1972) 77.
[9] R.E. Ansorge et al., Nucl. Phys. B63 (1973) 93.
[10] W. Gage et al., Nucl. Phys. B46 (1972) 21.
[11] K.G. Boreskov et al., Yad. Fiz. 15 (1972) 557; Sov. J. Nucl. Phys. 15 (1972) 309; A.P. Gasparyan et al., Yad. Fiz. 12 (1970) 987; Sov. J. Nucl. Phys. 12 (1971) 539.
[12] D. Lissauer et al., Phys. Rev. D6 (1972) 1852.
[13] H.H. Bingham et al., Diffractive dissociation of neutrons in π^-d interactions at 15 GeV/c, Paper submitted to the 2nd Aix-en-Provence Conf. on elementary particles, September 1973.
[14] H.I. Miettinen and P. Pirilä, Phys. Letters 40B (1972) 127.
[15] G.L. Kane, Acta Phys. Pol. B3 (1972) 845.
[16] J.C. Vander Velde et al., Nucl. Phys. B45 (1972) 1.
[17] Particle Data Group, Rev. Mod. Phys. 45 (1973) S1, p. 119.